FULL-FIELD SOLUTION FOR AN ANTIPLANE SHEAR CRACK IN ELASTIC MATERIALS WITH MICROSTRUCTURES

E. Radi

Dipartimento di Scienze e Metodi dell'Ingegneria, Università di Modena e Reggio Emilia, via Amendola 2 - 42100 Reggio Emilia, e-mail: eradi@unimore.it

SOMMARIO

In questo lavoro si studia il problema di una frattura semillimitata in condizioni di Modo III in un mezzo elastico caratterizzato dalla presenza di microstruttura. Il comportamento del materiale viene rappresentato attraverso il modello costitutivo elastico micropolare sviluppato da Koiter. Il modello considerato include le lunghezze caratteristiche a flessione e a torsione, proprie della microstruttura del materiale, e risulta pertanto in grado di simulare i rilevanti effetti di scala che si riscontrano in prossimità dell'apice di una frattura nei materiali con microstruttura, a distanze comparabili alle lunghezze caratteristiche. I campi di tensione e spostamento risultano notevolmente influenzati dal rapporto tra le lunghezze caratteristiche. In particolare, le tensioni tangenziali davanti all'apice a distanza inferiore alla lunghezza caratteristica a torsione, risultano di segno opposto rispetto alla soluzione elastica classica, a causa della rotazione relativa tra le particelle materiali situate in corrispondenza dell'apice. La soluzione completa mostra che la zona in cui si verifica tale inversione ha un'estensione molto ridotta e tende ad annullarsi con la lunghezza caratteristica a torsione del materiale. Al di fuori di tale zona, la tensione tangenziale assume un valore massimo, positivo e limitato. Tale valore può adottarsi come misura del livello critico di tensione necessario per far propagare la frattura. Il manifestarsi di un profilo di frattura a cuspide rivela inoltre che la tenacità a frattura dei materiali con microstruttura è in generale più elevata di quella dei materiali elastici classici, indicando quindi che la presenza di microstruttura può inibire il processo di frattura.

ABSTRACT

The present work deals with the problem of a stationary semi-infinite crack in an elastic solid with microstructures subect to remote classical K_{III} field. The material behaviour is described by the indeterminate theory of couple stress elasticity. By incorporating the characteristic lengths in bending and torsion of the material, the adopted constitutive model is able to account for the underlying micro-structure as well as for the strong size effects arising at small scales. The stress and displacement fields turn out to be strongly influenced by the ratio between the characteristic lengths. In particular, due to the relative rotation of the microstructural particles currently at the crack tip the total shear stress and reduced tractions ahead of the crack tip display the opposite sign with respect to the classical LEFM solution within a zone smaller than the characteristic length in torsion. However, this zone has limited physical relevance and becomes vanishing small for a characteristic length in torsion of zero. Outside this zone, the full field solution exhibits a bounded maximum for the shear stress ahead of the crack tip, whose magnitude can be adopted as a measure of the critical stress level for crack advancing. The corresponding fracture criterion defines a critical stress intensity factor which increases with the characteristic length in torsion. Moreover, the occurrence of a sharp crack profile indicates that the crack becomes stiffer with respect to the classical elastic response, thus revealing that the presence of microstructures may shield the crack tip from fracture.

1. INTRODUCTION

The main reason motivating the extension of the classical theory of elasticity to couple stress (CS) and strain gradient (SG) constitutive models is that the former is not able to characterize the constitutive behavior of brittle materials at the micron scale, due to the lack of a length scale. In particular, it can not predict the size effect experimentally observed when the representative scale of the deformation field becomes comparable to the length scale of the microstructure, such as the grain size in a polycrystalline or granular aggregate. It is well known indeed that in presence of stress concentration, such as near holes and notches, the macroscopic strength of these materials is higher if the grain size is smaller and that the bending and torsional strengths of beams and wires are greater if their cross section is thinner [1, 2]. In general, the size and shape of the microstructures have a strong influence on the mechanical properties of materials. The indeterminate theory of CS elasticity developed by Koiter [3] may be considered as an effort to include material characteristic lengths into the continuum theory. It allows accounting for the size and kind of microstructures since it involves two material parameters, namely the length ℓ and ratio η, which are related to the characteristic lengths in bending and torsion. As a consequence, CS elasticity can describe the mechanical behaviour of many materials with microstructures, like fibrous composites [4], cellular materials [5] and laminates, where moments may be transmitted through fibers, or in the cell ribs or walls. Also masonry, bone, foam and granular materials can be modelled within the framework of CS elasticity [6-8].

If the classical theory of elasticity is adopted for the analysis of the stress and deformation fields near the tip of a crack in a material with microstructures, then the results are expected to be rather inaccurate at distance to the crack tip comparable with the material characteristic lengths. Therefore, for the investigations of the crack tip fields at the micron scale it becomes necessary to make use of enhanced constitutive models, which may account for the presence of microstructure. The theory of CS elasticity may be considered as sufficiently accurate for the investigation of the crack tip zone and still enough simple to allow obtaining closed form analytical solutions.

The effects of elastic strain gradients on the stress and displacement fields for a stationary Mode III crack were investigated in [9-11]. In particular, the specialization of the constitutive model here adopted with $\eta = 0$ is considered in [9]. The results therein provided predict a substantial increase in the singularities of the skew-symmetric stress and couple stress fields, whereas the symmetric stress field turns out to be non-singular. Moreover, the shear stress and the reduced tractions ahead of the crack tip, within a zone smaller than the characteristic lengths, switch their sign with respect to the classical LEFM solution. This circumstance is due to the relative rotation of the particles currently at the crack tip, which yields opposite displacements ahead and behind the crack tip. The asymptotic analysis previously performed [12] for CS elastic material with two characteristic lengths confirmed this trend and showed that the angular distribution of the crack tip fields are strongly influenced by the characteristic lengths ratio η. A similar trend but with a reduced value of the singularity is also observed for Mode III crack propagation in elastic-plastic CS materials with linear strain hardening [13-14].

While the effects of the characteristic length in bending on Mode III crack fields have been investigated in [9], the role played by the characteristic length in torsion, which affects the ratio η but has no influence on ℓ, is almost unexplored. However, it is expected to have a strong influence on antiplane problems. Therefore, the problem of a stationary Mode III crack in a CS elastic solid with two characteristic lengths has been investigated in the present work. The full-field solution for a semi infinite crack subect to remote classical K_{III} field has been analytically obtained by following the approach introduced in [15] and later adopted in [9], which makes use of Fourier transform and Wiener-Hopf technique [16]. The knowledge of the full-field solution allows evaluating the size of the zone ahead of the crack tip where the shear stress has the negative sign, which is expected to strongly depend on the characteristic length in torsion and thus on the ratio η. Outside this zone, which has limited physical relevance, the shear stress is found to exhibit a bounded positive maximum. This occurrence allows formulating a fracture criterion for crack advancing which assumes a critical value for the maximum positive shear stress ahead of the crack tip. Correspondingly, the proposed criterion defines a critical value of the stress intensity factor required for crack propagation, which explicitly depends on the microstructure through the material characteristic lengths.

2. GOVERNING EQUATIONS

Reference is made to a Cartesian coordinate system (0, x_1, x_2, x_3) centred at the crack-tip. Under anti-plane shear deformation, the indeterminate theory of CS elasticity [3] adopted in the present study provides the following kinematical compatibility conditions between the out-of-plane displacement w, rotation vector $\boldsymbol{\varphi}$, strain tensor $\boldsymbol{\varepsilon}$ and deformation curvature tensor $\boldsymbol{\chi}$

$$\varepsilon_{13} = w_{,1}/2, \qquad \varepsilon_{23} = w_{,2}/2, \qquad \varphi_1 = w_{,2}/2, \qquad \varphi_2 = -w_{,1}/2, \tag{1}$$

$$\chi_{11} = -\chi_{22} = w_{,12}/2, \qquad \chi_{21} = -w_{,11}/2, \qquad \chi_{12} = w_{,22}/2. \tag{2}$$

Therefore, rotations are derived from displacements and the tensor field $\boldsymbol{\chi}$ turns out to be irrotational. According to the CS theory [3] the non-symmetric Cauchy stress tensor $\mathbf{t}$ can be decomposed into a symmetric part $\boldsymbol{\sigma}$ and a skew-symmetric part τ, namely $\mathbf{t} = \boldsymbol{\sigma} + \tau$. In addition, the couple stress tensor $\boldsymbol{\mu}$ is introduced as the work-conugated quantity of $\boldsymbol{\chi}^T$. For the antiplane problem within the CS theory $\boldsymbol{\varepsilon}$, $\boldsymbol{\sigma}$, τ, $\boldsymbol{\chi}$ and $\boldsymbol{\mu}$ are purely deviatoric tensors. The conditions of quasistatic equilibrium of forces and moments write

$$\sigma_{13,1} + \sigma_{23,2} + \tau_{13,1} + \tau_{23,2} = 0, \qquad \mu_{11,1} + \mu_{21,2} + 2\,\tau_{23} = 0, \qquad \mu_{12,1} + \mu_{22,2} - 2\,\tau_{13} = 0. \tag{3}$$

Within the context of small deformations theory, the total strain $\boldsymbol{\varepsilon}$ and the deformation curvature $\boldsymbol{\chi}$ are related to stress and couple stress through the following constitutive relations

$$\boldsymbol{\sigma} = 2G\,\boldsymbol{\varepsilon}, \qquad \boldsymbol{\mu} = 2G\,\ell^2\,(\boldsymbol{\chi}^T + \eta\,\boldsymbol{\chi}), \tag{4}$$

where G is the elastic shear modulus, ν the Poisson ratio, ℓ and η the CS parameters introduced in [3], with $-1 \quad \eta \quad 1$. The material parameters ℓ and η depend on the material characteristic lengths in bending and in torsion, namely $\ell_b = \ell/\sqrt{2}$ and $\ell_t = \ell\,(1+\eta)^{1/2}$. Typical values of ℓ_b and ℓ_t for some classes of materials with microstructure can be found in [6-7]. In particular, the limit value of $\eta = -1$ corresponds to a vanishing small characteristic length in torsion, typical of polycrystalline metals, and the case $\eta = 0$ studied in [9], corresponds to $\ell_t = \ell = \sqrt{2}\,\ell_b$. Constitutive equations (4) and compatibility relations (1) and (2) give stresses and couple stresses as functions of the displacement w:

$$\sigma_{13} = G\,w_{,1}, \qquad \sigma_{23} = G\,w_{,2}, \tag{5}$$

$$\mu_{11} = \mu_{22} = G\,\ell^2\,(1+\eta)\,w_{,12}, \qquad \mu_{21} = G\,\ell^2\,(w_{,22} - \eta\,w_{,11}), \qquad \mu_{12} = -G\,\ell^2\,(w_{,11} - \eta\,w_{,22}). \tag{6}$$

The introduction of (6) into $(3)_{2,3}$ yields

$$\tau_{13} = -G\,\ell^2\,\Delta w_{,1}/2, \qquad \tau_{23} = -G\,\ell^2\,\Delta w_{,2}/2, \tag{7}$$

where Δ denotes the Laplace operator. A substitution of (7) and (5) into $(3)_1$ gives the following PDE for the function w:

$$2\,\Delta w - \ell^2\,\Delta\Delta w = 0. \tag{8}$$

The reduced tractions p_3 and couple stress tractions q_1 on the crack surfaces are

$$p_3 = \sigma_{23} + \tau_{23} + \mu_{22,1}/2 = 0, \qquad q_1 = \mu_{21} = 0, \tag{9}$$

respectively. According to $(5)_2$, $(6)_{1,2}$ and $(7)_2$, vanishing of generalized tractions (9) on the crack surface implies the following boundary conditions for the function w:

$$2\,w_{,2} - \ell^2\,[(2+\eta)\,w_{,11} + w_{,22}]_{,2} = 0, \qquad w_{,22} - \eta\,w_{,11} = 0, \qquad \text{for } x_1 \quad 0, \quad x_2 = 0. \tag{10}$$

Moreover, ahead of the crack tip the skew-symmetry of the Mode III crack problem requires

$$w = 0, \qquad w_{,22} - \eta\,w_{,11} = 0, \qquad \text{for } x_1 \quad 0, \quad x_2 = 0. \tag{11}$$

3. FULL FIELD SOLUTION

In the present section the Wiener-Hopf analytic continuation technique [16] is used to obtain the full field solution for a semi infinite crack in an infinite medium subect to remote classical K_{III} field. Only the upper half-plane ($x_2 \geq 0$) is considered due to the skew-symmetry of the problem. Use of the Fourier transform and inverse transform is made. For the function $w(x_1, x_2)$ they are

$$\overline{w}(s, x_2) = \int_{-\infty}^{\infty} w(x_1, x_2)\,e^{isx_1}\,dx_1, \qquad w(x_1, x_2) = \frac{1}{2\pi}\int_{-\infty}^{\infty} \overline{w}(s, x_2)\,e^{-isx_1}\,ds, \tag{12}$$

respectively, where s is a real variable. Introduction of $(12)_2$ into the governing equation (8), yields the

following ODE for $\overline{w}(s, x_2)$

$$\overline{w}_{,2222} - 2\,(s^2 + 1/\ell^2)\;\overline{w}_{,22} + s^2\,(s^2 + 2/\ell^2)\;\overline{w} = 0, \tag{13}$$

which admits as bounded solution in the upper half-plane

$$\overline{w}\,(s, x_2) = C(s)\;e^{-\sqrt{s^2+2/\ell^2}\,x_2} + D(s)\;e^{-|s|x_2}, \qquad \text{for } x_2 \geq 0, \tag{14}$$

where the functions $C(s)$ and $D(s)$ can be determined by the boundary conditions (10) and (11). Introduction of $(12)_2$ and (14) into the boundary conditions $(10)_2$ and $(11)_2$, which hold on the entire line $x_2 = 0$, yields the following relation between $C(s)$ and $D(s)$

$$C(s) = -\frac{\alpha\, s^2}{1 + \alpha\, s^2}\;D(s), \qquad \text{where} \qquad \alpha = (1+\eta)\;\ell^2/2, \tag{15}$$

and thus the function $\overline{w}$ in (14) can be written as:

$$\overline{w}\,(s, x_2) = [\,e^{-|s|x_2} - \frac{\alpha\, s^2}{1 + \alpha\, s^2}\;e^{-\sqrt{s^2+2/\ell^2}\,x_2}\,]\;D(s), \qquad \text{for } x_2 \geq 0. \tag{16}$$

The Fourier transform of the boundary condition $(10)_1$, yields

$$\overline{w}_{,2}\,(s, 0) + [(2 + \eta)\;s^2\;\overline{w}_{,2}\,(s, 0) - \overline{w}_{,222}\;(s, 0)]\;\ell^2/2 \;=\; \overline{p}_{3+}(s)\,/G, \tag{17}$$

where $\overline{p}_{3+}$ is the transform of the reduced traction p_3 ahead of the crack tip, at x_1 0 and $x_2 = 0$:

$$\overline{p}_{3+}(s) = G\int_0^{\infty}\{w_{,2}(x_1, 0) - \frac{\ell^2}{2}[(2 + \eta)\;w_{,112}(x_1, 0) + w_{,222}(x_1, 0)\,]\}\;e^{isx_1}\,dx_1, \tag{18}$$

which is analytic in the upper half complex s plane, $\mathrm{Im}(s)$ 0. Similarly, the Fourier transform of the boundary condition $(11)_1$ which applies to x_1 0 only, gives

$$\overline{w}\,(s, 0) \;=\; \overline{w}_{-}\,(s), \qquad \text{where} \qquad \overline{w}_{-}\,(s) = \int_{-\infty}^{0} w(x_1, 0)\;e^{isx_1}\,dx_1, \tag{19}$$

is analytic in the lower half complex s plane, $\mathrm{Im}(s)$ 0. Introduction of (14) and (15) in (17) and (1 9) gives

$$\overline{p}_{3+}(s) = G\,[\frac{(\alpha\, s^2)^2}{1 + \alpha\, s^2}\,(s^2 + 2/\ell^2)^{1/2} - (1 + \alpha\, s^2) \quad s\,]\;D(s), \qquad \overline{w}_{-}\,(s) = D(s)\,/(1 + \alpha\, s^2), \tag{20}$$

respectively. Elimination of $D(s)$ from (20) yields

$$\overline{p}_{3+}(s) = -\,G \quad s \quad f\,(s)\;\overline{w}_{-}\,(s), \qquad \text{where} \qquad f\,(s) = (1+\alpha\, s^2)^2 - \alpha\, s^2\,(\alpha\, s^2)^{1/2}\,(1+\eta+\alpha\, s^2)^{1/2}. \tag{21}$$

In order to apply to the Wiener–Hopf technique of analytic continuation, equation $(21)_1$ needs to be factorized into the product of two functions analytic in the upper and lower half s planes, respectively. Note that the function s can be factorized as $s = s_+^{1/2}\,s_-^{1/2}$, where $s_+^{1/2}$ and $s_-^{1/2}$ have branch cuts from 0 to $-i\infty$ and from 0 to $i\infty$, and are therefore analytic in the upper and lower half s planes, respectively. The branch cuts are chosen such that the square root functions are positive when s is real and positive. By using the argument principle [15] it can be shown that the function $f\,(s)$ has only two roots in the complex s plane, namely $s = \quad i\,a\,\alpha^{-1/2}$, where a is the unique real and positive, non-dimensional root of the equation

$$(3 - \eta)\;a^6 - 6\;a^4 + 4\;a^2 - 1 = 0, \tag{22}$$

Note that a 1 for $\eta = 0$. The function $f\,(s)$ can thus be factorized by following the approach proposed in [14] and [9] as

$$f\,(s) = \frac{3 - \eta}{2}\;(\alpha\, s^2 \;+ a^2)\;k_{-}(s)\;k_{+}(s), \tag{23}$$

where the functions

$$k_{+}(s) = e^{-R(-is\ell/\sqrt{2})}, \qquad k_{-}(s) = e^{-R(is\ell/\sqrt{2})}, \tag{24}$$

are analytic in the upper and lower half complex s planes, respectively, and the function R is

$$R(x) = \frac{1}{\pi} \int_0^1 arctg\left[\frac{t^3\sqrt{1-t^2}}{(\frac{1}{1+\eta} - t^2)^2}\right] \frac{dt}{t+x}. \tag{25}$$

By multiplying both sides of equation $(21)_1$ by s and using (23), it can be factorized as

$$\frac{4}{(3-\eta)(1+\eta)G\ell^2} \frac{\overline{p}_{3+}(s)\, s_+^{1/2}}{(s + i\,a/\sqrt{\alpha})\, k_+(s)} = -s_-^{3/2}\ (s - i\,a/\sqrt{\alpha}\,)\ k_-(s)\ \overline{w}_-(s). \tag{26}$$

The left and right sides of (26) are analytic functions in the upper and lower half s plane, respectively, and thus define an entire function on the s plane. The Fourier transform of the asymptotic fields obtained in Section 3 gives $\overline{p}_{2+} \sim s^{1/2}$ and $\overline{w}_- \sim s^{-5/2}$ as $s \to \infty$, and thus both sides of (26) are bounded as $s \to \infty$ and must equal a constant F in the entire s plane according to Louville's theorem, so that

$$\overline{p}_{3+}(s) = (1+\eta)(3-\eta)\frac{F\,G\,\ell^2}{4} \frac{(s + i\,a/\sqrt{\alpha})\, k_+(s)}{s_+^{1/2}}, \qquad \overline{w}_-(s) = -\frac{F}{s_-^{3/2}(s - i\,a/\sqrt{\alpha})\, k_-(s)}. \tag{27}$$

The constant F can be determined from the Fourier transform of the remotely applied classical K_{III} field, namely for $r \to \infty$, which corresponds to $s \to 0$. The Fourier transform of sliding displacement and shear stress in classical K_{III} field are

$$\overline{p}_{3+}(s) = \frac{1+i}{2\, s_+^{1/2}} K_{III}, \qquad \overline{w}_-(s) = -\frac{1+i}{2\,G\, s_-^{3/2}} K_{III}, \quad \text{as } s \to 0. \tag{28}$$

A comparison of (28) with the limit of (27) as $s \to 0$, by using $(21)_2$, (23) and (24), implies that

$$F = \frac{K_{III}}{G\,\ell} \frac{1-i}{\sqrt{(1+\eta)(3-\eta)}}. \tag{29}$$

Finally, the introduction of (29) and (24) in (27) yields

$$\overline{w}_-(s) = -\frac{K_{III}}{G\,\ell} \frac{1-i}{\sqrt{(1+\eta)(3-\eta)}} \frac{e^{R(i\,s\,\ell/\sqrt{2})}}{s^{3/2}\,(s - i\,a/\sqrt{\alpha})}, \tag{30}$$

$$\overline{p}_{3+}(s) = K_{III}\,\ell \frac{1-i}{4} \sqrt{(1+\eta)(3-\eta)}\ [(s)^{1/2} + i\,a\,(\alpha\, s)^{-1/2}]\, e^{-R(-i\,s\,\ell/\sqrt{2})}. \tag{31}$$

4. RESULTS

Stress, couple stress and displacement fields can be obtained from (30) and (31) by inverse Fourier transform. In particular, the Fourier transform of the total shear stress $t_{23} = \sigma_{23} + \tau_{23}$ at $x_2 = 0$ follows from $(5)_2$, $(7)_2$, (17), $(21)_2$ and (31) as:

$$\bar{t}_{23}(s, 0) = K_{III}\,\ell \frac{1-i}{2} \sqrt{\frac{1+\eta}{3-\eta}} \frac{(1+\alpha\, s^2)\, e^{R(i\,s\,\ell/\sqrt{2})}}{(\sqrt{\alpha}\, s - i\,a)\,(\alpha\, s)^{1/2}}. \tag{32}$$

The integration path in the inverse Fourier transform may be transformed in the lower half s plane to two straight lines on the two sides of the negative imaginary axis plus a half circle centered at the origin with radius approaching infinity. The integration on the large circle then gives a vanishing small contribution, whereas the integration over the two straight lines yields

$$t_{23}(x_1, 0) = \frac{K_{III}\sqrt[4]{2}}{\pi\sqrt{(3-\eta)\,\ell}} \int_0^\infty e^{-\sqrt{2}\,t\,x_1/\ell} \frac{1 - t^2(1+\eta)}{[a + t\sqrt{1+\eta}\,]\sqrt{t}}\, e^{R(t)}\, dt, \text{ for } x_1 \quad 0. \tag{33}$$

The normalized shear stress ahead of the crack tip, $t_{23}(2\pi\ell)^{1/2}/K_{III}$ at $x_2 = 0$, versus normalized distance x_1/ℓ is shown in Fig. 1a, together with the near-tip asymptotic field for CS elasticity obtained in [12] and the shear stress traction in the classical K_{III} field. The full-field solution displays a smooth transition from the positive remote classical K_{III} field to the negative near-tip field, as x_1 decreases and becomes smaller than ℓ. As the ratio η decreases from 1 to −1 and thus ℓ_t tends to zero, then the total shear

stress t_{23} approaches the classical K_{III} field from below. However, it switches to negative values at very small distance to the crack tip, denoted by x_1^0. The variation of the ratio x_1^0/ℓ with η is plotted in Fig. 1b (dash-dotted line). It can be observed that the zone ahead of the crack tip with negative shear stress significantly reduces in size and tends to vanish as η comes close to −1, as a consequence of the corresponding reduction in the characteristic length in torsion ℓ_t. Strain gradient effects are observed up to a distance of 5ℓ to the crack tip. For larger distance the full-field solution coincides with the classical K_{III} field.
Since the size of the zone where the shear stress has the negative sign is very small, it can be considered of no physical importance. Outside of this zone the shear stress exhibits a maximum that is bounded and positive for −1 η 1. The maximum is attained at a distance x_1^{max} to the crack tip, which satisfy the condition $t_{23,1}(x_1^{max}, 0) = 0$, namely from (33):

$$\int_0^\infty e^{-\sqrt{2}\,t\,x_1^{\max}/\ell}\,\frac{1-t^2(1+\eta)}{[a+t\sqrt{1+\eta}\,]}\,\sqrt{t}\;e^{R(t)}\;dt\;=0. \tag{34}$$

The variation of the non dimensional ratio x_1^{max}/ℓ is plotted in Fig. 1b as function of η (dashed line). Classical LEFM does not provide this feature since the classical K_{III} shear stress field monotonically increases and is unbounded without any local maximum (Fig. 1a). The occurrence of a maximum positive value of the shear stress ahead of the crack tip, $t_{23}^{max} = t_{23}(x_1^{max}, 0)$, allows formulating a simple fracture criterion by assuming a critical shear stress level τ_C at which the crack may start propagating. The corresponding fracture criterion may thus be written as $t_{23}^{max} = \tau_C$. The normalized value of t_{23}^{max} is plotted in Fig. 1b as a function of η (dotted line). It is unbounded as η approaches −1, since in this limit the full field solution for the total shear stress approaches the classical K_{III} field, and it decreases as η increases from −1 to 1, in agreement with the results plotted in Fig. 1a. According to the proposed fracture criterion, a critical stress intensity factor K_{IIIC} can be defined by using (33) as

$$K_{IIIC} = \tau_C\,\frac{\pi\sqrt{(3-\eta)\,\ell}}{\sqrt[4]{2}}\int_0^\infty e^{-\sqrt{2}\,t\,x_1^{\max}/\ell}\,\frac{1-t^2(1+\eta)}{[a+t\sqrt{1+\eta}\,]\,\sqrt{t}}\,e^{R(t)}\,dt\,. \tag{35}$$

The normalized value of K_{IIIC} is plotted in Fig. 1b as a function of η (solid line). It explicitly depends on the microstructure through the parameters ℓ and η and, in particular, it is found to increase with η. It follows that materials with larger characteristic length in torsion are expected to exhibit higher fracture toughness under Mode III loading conditions, in agreement with previous investigations [5, 11], which also found that the presence of microstructure yields an increase of fracture toughness.
The sliding displacement w on the crack face can be obtained from the inverse Fourier transform of equation (30). However, in order to ensure the inverse Fourier transform converges the function $w_{,1}$ is first obtained from the inverse Fourier transform of $-i\,s\,\overline{w}_-$, Then, a conversion of the integration path to the positive imaginary s axis, where $s = iy$ and $y \geq 0$, yields:

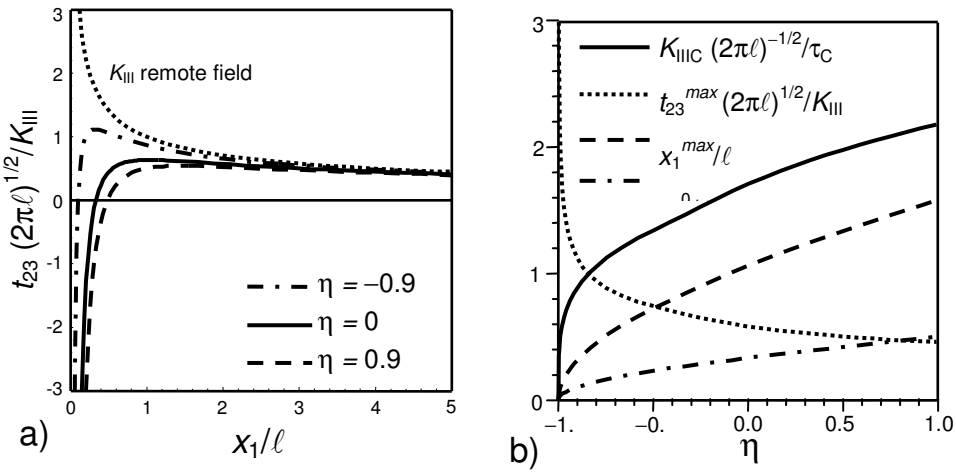

Fig. 1 – a) variation of shear stress t_{23} along the x_1 axis, ahead of the crack tip. b) variations of the critical stress intensity factor K_{IIIC}, maximum shear stress t_{23}^{max} and its location x_1^{max} and size x_1^0 of the

zone with negative shear stress with the ratio η

$$w_{,1}(x_1, 0) = \frac{K_{\mathrm{III}}}{G\,\ell}\,\frac{\sqrt{2}}{\pi\sqrt{(1+\eta)(3-\eta)}}\int_0^{\infty}\frac{e^{R(-y\ell/\sqrt{2})+y\,x_1}}{\sqrt{y}\;(y-a/\sqrt{\alpha})}\,dy, \quad \text{for } x_1 \;\; 0. \tag{36}$$

By integrating $w_{,1}$ with respect to x_1, imposing the condition $w = 0$ at the crack tip, namely at $x_1 = 0$ and substituting for $t = y\ell/\sqrt{2}$, the displacement on the crack surface can be obtained as

$$w\,(x_1, 0) = \frac{K_{\mathrm{III}}}{\sqrt[4]{2}\;G}\,\frac{\sqrt{\ell}}{\pi\sqrt{(1+\eta)(3-\eta)}}\int_0^{\infty}\frac{(e^{\sqrt{2}\,t\,x/\ell}-1)\,e^{R(-t)}}{t\,\sqrt{t}\;(t-\frac{a}{\sqrt{1+\eta}})}\,dt, \quad \text{for } x_1 \;\; 0. \tag{37}$$

By using $(21)_2$, (22), (23) and (24), it can be shown that

$$e^{R(-t)} = \frac{3-\eta}{2}\,\frac{(\frac{1}{1+\eta}-t^2)^2+t^2\sqrt{t^2}\sqrt{t^2-1}}{(3-\eta)\,t^4-\frac{4a^2-1}{a^4(1+\eta)}\,t^2+\frac{1}{a^2(1+\eta)^2}}\,e^{-R(t)}. \tag{38}$$

Finally, the introduction of equation (38) in the expression (37) of the sliding displacement yields

$$w\,(x_1, 0) = \frac{K_{\mathrm{III}}\sqrt{\ell}}{2^{5/4}\,\pi G}\sqrt{\frac{3-\eta}{1+\eta}}\int_0^{\infty}\frac{(e^{\sqrt{2}\,t\,x_1/\ell}-1)\,[(\frac{1}{1+\eta}-t^2)^2+t^3\sqrt{t^2-1}\;H(t-1)]\,dt}{t\,\sqrt{t}\;(t-\frac{a}{\sqrt{1+\eta}})\,[(3-\eta)\,t^4-\frac{4a^2-1}{a^4(1+\eta)}\,t^2+\frac{1}{a^2(1+\eta)^2}]\,e^{R(t)}}, \tag{39}$$

for $x_1 \;\; 0$, where the Cauchy principal value of the integr al must be considered, since the integrand function is singular at $t = a\,(1+\eta)^{-1/2}$.

The normalized sliding displacement on the crack face, $w\,G\,(\pi/2\ell)^{1/2}/K_{\mathrm{III}}$ at $x_2 = 0$, versus normalized distance r/ℓ to the crack tip is shown in Fig. 2a and plotted in logarithmic scales in Fig. 2b. As well known, the crack tip profile is blunted for the classical K_{III} displacement field whereas it turns out to be sharp in CS elastic materials, in agreement with the atomistically sharp crack tip experimentally observed for cleavage fracture [17]. The magnitude of the sliding displacement between the crack faces remarkably decreases as η increases from −1 to 1, indicating that the crack becomes stiffer in comparison with the classical elastic response. In fact, the strain energy density for CS materials increases with respect to classical elasticity due to the contribution of the strain rotational gradients, thus resulting in a stiffer material. This occurrence confirms that the microstructure may shield the crack tip from fracture, as already observed in [11] for SG elastic behavior and in [13, 14] for Mode III ductile crack propagation in materials with microstructures.

The dotted straight lines with slopes 3/2 in Fig. 2b correspond to the near-tip asymptotic field for CS elasticity obtained in [12] for the three considered values of η, whereas the dotted line with slope 1/2 corresponds to the classical solution of LEFM under K_{III} remote field. From Fig. 2b it can be observed that the full-field solution displays a smooth transition between these two fields.

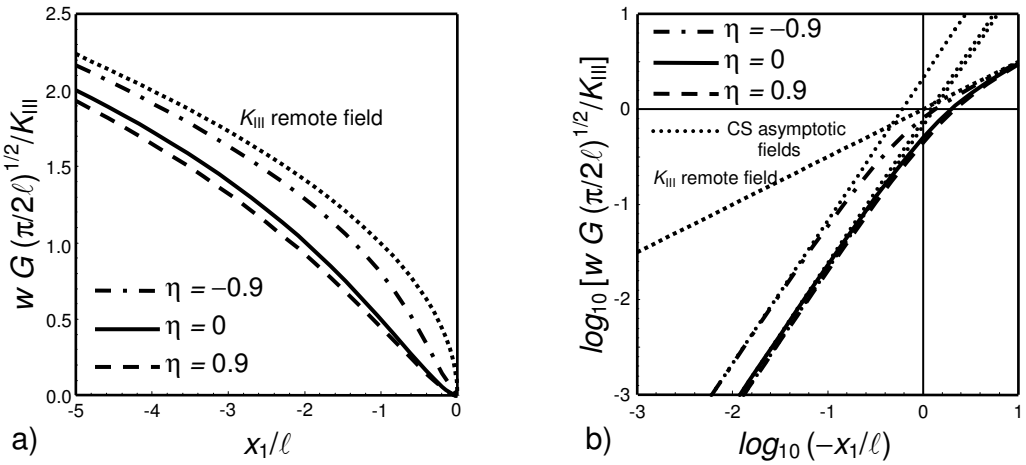

Fig. 2. Variation of crack face sliding displacement w along the crack face.

5. CONCLUSIONS

The full-field solution here provided for a semi-infinite mode III crack in CS elastic materials with characteristic lengths in bending and torsion sube ct to remote classical K_{III} field displays a continuous transition from the classical K_{III} fields, which hold at a distance to the crack tip larger than 5ℓ, to the asymptotic fields which display negative shear stress ahead of the crack tip. The size of the zone with negative shear stress tends to vanish as η approaches the limit value -1, which corresponds to a vanishing small characteristic length in torsion. Outside this extremely small zone, which actually has no physical relevance, the total shear stress distribution exhibits a local bounded maximum, whose magnitude can be adopted as a measure of the critical stress level for further crack advancing. According to this fracture criterion the fracture toughness of the material is shown to increases with the characteristic length in torsion. The occurrence of a sharp crack profile also indicates that the crack becomes stiffer with respect to the classical elastic response, thus revealing that the presence of microstructures may shield the crack tip from fracture. Shielding can reasonably be expected since the contribution of strain gradients to the strain energy density increases the stiffness of the material.
As a conclusion, the present approach provides a means to link scales in fracture mechanics, namely from atomistic through microscale to macroscopic fracture, which allows understanding the detailed mechanisms by which fracture may occur in brittle materials with complex microstructure, up to the micron scale. Moreover, the inclusion of two material characteristic lengths provides more realistic predictions on the tractions level ahead of the crack-tip then the classical LEFM solution, as well as more accurate results then the simple CS theory of elasticity with $\eta = 0$ adopted in [9]. It also sheds some light on the shielding mechanisms against fracture originating from the presence of microstructures and allows evaluating the corresponding increase in Mode III fracture toughness.

REFERENCES

[1] Gauthier RD, Jahsman WE. A quest for micropolar elastic constants. Journal of Applied Mechanics. 1975; 42: 369-374.
[2] Fleck NA, Muller GM, Ashby MF, Hutchinson JW. Strain gradient plasticity, theory and experiment. Acta Metallurgica et Materialia. 1994; 42: 475-487.
[3] Koiter WT. Couple-stresses in the theory of elasticity, I and II. Proc. Kon. Nederl. Akad. Wetensch (B) 1964; 67: 17-44.
[4] Hlavacek M. A continuum theory for fibre reinforced composites. International Journal of Solids and Structures 1975; 11:199-211.
[5] Chen J , Huang , Ortiz M. Fracture of cellular materials, a strain gradient model. Journal of the Mechanics and Physics of Solids 1998; 46: 789–828.
[6] Lakes RS. Experimental microelasticity of two porous solids. International Journal of Solids and Structures. 1986; 22: 55-63.
[7] Lakes RS. Experimental methods for study of Cosserat elastic solids and other generalized elastic continua. In: M hlhaus H, (Ed.), Continuum models f or materials with micro-structure. John Wiley, New ork, 1995; pp. 1-22.
[8] Casolo S. Macroscopic modelling of structured materials: Relationship between orthotropic Cosserat continuum and rigid elements. International Journal of Solids and Structures 2006; 43: 475-496.
[9] hang L, Huang , Chen J , Hwang KC. The Mode I II full-field solution in elastic materials with strain gradient effects. International Journal of Fracture. 1998; 92: 325-348.
[10] Fanniang AC, Chan S, Paulino GH. Strain grad ient elasticity for antiplane shear cracks, a hypersingular integrodifferential equation approach. SIAM Journal of Applied Mathematics. 2002; 62, 1066-1091.
[11] Georgiadis, H.G., 2003. The Mode III crack problem in microstructured solids governed by dipolar gradient elasticity, static and dynamic analysis. Journal of Applied Mechanics 70, 517-530.
[12] Radi E. Mode III crack tip fields in couple stress elastic materials with two characteristic lengths. IGF 18 - VIII Convegno Nazionale Gruppo Italiano F rattura. Cetraro (CS), 31/05-1/06/2006.
[13] Radi E. Effects of characteristic material lengths on mode III crack propagation in couple stress elastic-plastic materials. International Journal of Plasticity. 2007; 23: 1439-1456.
[14] Radi E, Gei M. Mode III crack growth in linear hardening materials with strain-gradient effects. International Journal of Fracture. 2004; 130: 765-785.
[15] Atkinson C, Leppington FG. The effect of couple stresses on the tip of a crack. International Journal of Solids and Structures. 1977; 13: 1103-1122.
[16] Freund LB. Dynamic fracture mechanics. Cambridge: Cambridge University Press, 1990.

[17] Elssner G, Korn D, Ruehle M. The influence of interface impurities on fracture energy of UHV diffusion bonded metal-ceramic bicrystals. Scripta Metallurgica et Materialia. 1994; 31:1037-1042.